



Published in final edited form as:

Medchemcomm. 2013 January 1; 4(1): 112–119. doi:10.1039/C2MD20127E.

Inhibitors of bacterial tubulin target bacterial membranes *in vivo*†

Marie H. Foss^a, Ye-Jin Eun^a, Charles I. Grove^b, Daniel A. Pauw^c, Nohemy A. Sorto^b, Jarred W. Rensvold^a, David J. Pagliarini^a, Jared T. Shaw^b, and Douglas B. Weibel^{a,d}

Douglas B. Weibel: weibel@biochem.wisc.edu

^aDepartments of Biochemistry and Biomedical Engineering, 433 Babcock Drive, Madison, WI 53706, USA. Tel: +1 (608) 890-1342

^bDepartment of Chemistry, University of California-Davis, Davis, CA 95616, USA

^cDepartment of Cell and Molecular Biology, University of Wisconsin– Madison, Madison, WI 53706, USA

^dDepartment of Biomedical Engineering, University of Wisconsin– Madison, Madison, WI 53706, USA

Abstract

FtsZ is a homolog of eukaryotic tubulin that is widely conserved among bacteria and coordinates the assembly of the cell division machinery. FtsZ plays a central role in cell replication and is a target of interest for antibiotic development. Several FtsZ inhibitors have been reported. We characterized the mechanism of these compounds in bacteria and found that many of them disrupt the localization of membrane-associated proteins, including FtsZ, by reducing the transmembrane potential or perturbing membrane permeability. We tested whether the reported phenotypes of a broad collection of FtsZ inhibitors disrupt the transmembrane potential in *Bacillus subtilis* strain 168. Using a combination of flow cytometry and microscopy, we found that zantrin Z1, cinnamaldehyde, totarol, sanguinarine, and viriditoxin decreased the *B. subtilis* transmembrane potential or perturbed membrane permeability, and influenced the localization of the membrane-associated, division protein MinD. These studies demonstrate that small molecules that disrupt membrane function in bacterial cells produce phenotypes that are similar to the inhibition of proteins associated with membranes *in vivo*, including bacterial cytoskeleton homologs, such as FtsZ. The results provide a new dimension for consideration in the design and testing of inhibitors of bacterial targets that are membrane-associated and provide additional insight into the structural characteristics of antibiotics that disrupt the membrane.

Introduction

The bacterial homolog of eukaryotic tubulin, FtsZ, performs the essential role of recruiting the cell division machinery to the mid-cell during replication.^{1,2} FtsZ binds GTP and assembles into filaments at the cytoplasmic membrane where it forms the Z-ring. The Z-ring marks the division plane and is the scaffold for the assembly of the cell division machinery. During division, the Z-ring contracts as the cell wall is remodelled and creates the septum, which physically separates mother and daughter cells. Loss of FtsZ function blocks division

†Electronic supplementary information (ESI) available: Supplemental methods and figures can be found in the supplemental information.

and leads to the formation of long, multi-nucleoid cells (*e.g.* filaments) *via* uncoupling growth and division.^{3,4} Several physiological mechanisms inhibit FtsZ directly and block cell division. For example, DNA damage initiates the SOS response and triggers expression of a protein antagonist of FtsZ, SulA (also called SfiA), which stalls division for DNA damage repair.^{5,6} Another mechanism is the inhibition of DNA replication, as the nucleoid occlusion machinery prevents the assembly of functional Z-rings in the presence of incompletely replicated chromosomal DNA.^{7,8} In sporulating *Bacillus subtilis*, the peptide MciZ halts cytokinesis in the mother cell by inhibiting FtsZ.⁹ The *B. subtilis* protein UgtP is involved in sensing growth conditions and inhibits FtsZ assembly until cells have an appropriate mass.⁴

The loss of the transmembrane potential ($\Delta\psi$) was recently reported as a negative regulator of FtsZ function.¹⁰ $\Delta\psi$ arises from the separation of different concentrations of charged ions across the bacterial membrane and can be measured using a permeable cationic dye and the Nernst equation (eqn (1)), where C_i is the concentration of the dye inside the cell and C_o is the concentration of dye outside, R is the gas constant, T is temperature, Z is the number of electrons per mole of dye, and F is the Faraday constant.¹¹

$$\Delta\Psi = -\frac{RT}{ZF} \ln \frac{C_i}{C_o} \quad (1)$$

$\Delta\psi$ is a source of potential energy that facilitates the transport of molecules and ions across the cell membrane. The establishment of the proton motive force (pmf) contributes significantly to $\Delta\psi$ and facilitates ATP production *via* oxidative phosphorylation.¹² The relationship between $\Delta\psi$ and the chemical proton potential can be described by eqn (2), where ΔpH is the difference between the internal and external pH ($\text{pH}_{\text{in}} - \text{pH}_{\text{out}}$).¹²

$$\text{pmf} = \Delta\Psi - \frac{2.3RT}{F} \Delta\text{pH} \quad (2)$$

A recently discovered role of $\Delta\psi$ is the localization of membrane-associated proteins, including bacterial proteins that regulate division and cell shape.¹⁰ Carbonyl cyanide *m*-chlorophenylhydrazone (CCCP, **1**, Table 1) is among the best-studied small molecules that shuttle protons across the membrane (*e.g.* ‘protonophores’) and affects the localization of several membrane-associated proteins, including the division protein FtsA;¹⁰ Fig. 1 illustrates an effect of $\Delta\psi$ on the localization of MinD. Small molecules that perturb $\Delta\psi$ may mislead the assignment of their target *in vivo*. Despite evidence that small molecules can influence the localization of division proteins *via* perturbing bacterial membranes, the effect of the relatively large number of putative inhibitors of this class of proteins on $\Delta\psi$ has not yet been studied.

FtsZ is among the most widely studied bacterial cytoskeletal proteins and is a central component of the cell division machinery. The essential role of FtsZ makes it a target of interest for the development of antibiotics. Consequently, several small molecule inhibitors of FtsZ have been reported and their target identification draws upon their activity *in vitro* and *in vivo*.^{13–21} The *in vivo* activity of several of these FtsZ inhibitors is centered upon two distinct observations: (1) cell filamentation; and (2) mislocalization of FtsZ. However, these experiments do not assess whether the inhibitor influences the properties of membranes, which provides the mechanism for mislocalizing membrane-associated proteins, such as FtsZ. An example is the proposed inhibitor of FtsZ, zantrin Z1, which we refer to as ‘3Z1’ or **2**.¹³ Although **2** delocalizes FtsZ and has a minimum inhibitory concentration (MIC) of 0.08–40 μM against a range of bacterial strains,²² treatment of *Escherichia coli* with this

small molecule (5 μM , or $1 \times \text{MIC}$) does not filament cells, which is the canonical phenotype of FtsZ inhibition. This result suggests that the activity of this compound is not due to inhibiting FtsZ *per se*. Many putative FtsZ inhibitors produce phenotypes that are unrelated to FtsZ inhibition and their physicochemical properties make them excellent candidates for interacting with phospholipid bilayers.

In reviewing proposed FtsZ inhibitors, we identified several compounds that may influence the properties of bacterial membranes. Cinnamaldehyde (**3**) is an antimicrobial agent that has been reported to inhibit FtsZ.¹⁴ The chemically related compound curcumin affects the activities of multiple disparate membrane proteins by changing lipid bilayer properties.²³ For example, curcumin thins bilayers and decreases their stiffness.^{23,24} Totarol (**4**) has been assigned several other functions *in vivo*, including: (1) inhibiting multidrug efflux pumps;²⁵ (2) inhibiting the bacterial electron transport chain;²⁶ and (3) disrupting the physical properties of the membrane.²⁷ Totarol has a large phospholipid-water partition coefficient ($K_p = 1.8 \times 10^4$) and is sequestered in membranes.²⁸ Sanguinarine (**5**) inhibits the activity of guinea pig cardiac Na^+ , K^+ -ATPase²⁹ and causes mitochondrial depolarization in mouse melanoma cells.³⁰ Viriditoxin (**6**) activates ATP hydrolysis and induces calcium sensitized swelling of rat liver mitochondria.³¹ A common feature of these compounds is their interaction with phospholipid membranes. Although these compounds may bind FtsZ *in vitro*, the mis-localization of membrane-associated proteins *in vivo* may be due to changes in the physicochemical properties of membranes that arise in response to the small molecules.

Several of these compounds share physicochemical characteristics with reported uncouplers of ΔpH and $\Delta\psi$; the compounds are lipophilic weak acids that contain electron-withdrawing groups.^{32,33} We sought to test the hypothesis that their effect on FtsZ and other membrane-associated proteins *in vivo* arises from disrupting $\Delta\psi$. We tested a panel of reported FtsZ inhibitors (Table 1) for their ability to deplete $\Delta\psi$ in *B. subtilis* 168 and determined whether the effect delocalized the cytoplasmic membrane-associated protein, MinD. In this paper we demonstrate that many of the small molecules identified as hits from various high-throughput screens against the bacterial protein FtsZ, depolarize the bacterial membrane and delocalize FtsZ non-specifically.

Results and discussion

Our primary motivation for evaluating putative FtsZ inhibitors for effects on membrane function and membrane-protein localization was two-fold: (1) to eliminate false-positives from the pool of available FtsZ inhibitors; and (2) to define chemical characteristics that target bacterial membranes. Small molecules that target membranes are currently being pursued for treating infections by slow or non-growing populations of bacteria³⁴ and may be useful adjuvants for existing classes of antimicrobial agents.³⁵

For our studies, we used MinD translationally fused to green fluorescent protein (GFP) as a model membrane-associated protein for several reasons. (1) MinD plays a role in bacterial cell division and regulation of FtsZ activity *in vivo*.^{36,37} (2) MinD contains a well-characterized terminal amphipathic helix that associates with the cytoplasmic membrane.³⁸ (3) MinD binds preferentially to anionic phospholipids, and the local organization of these lipids is thought to influence the position of the protein *in vivo*.^{39,40} In principle, disrupting $\Delta\psi$ should cause MinD to mislocalize *in vivo*. To test this hypothesis, we used *Bacillus subtilis* as a model Gram-positive bacterium. We chose *B. subtilis* because all the compounds we tested are reported to target FtsZ in Gram-positive cells; very few are active against Gram-negative bacteria. We tested compounds with broad-spectrum activity against *B. subtilis* 168 and *E. coli* MG1655.

The compounds used in this study included: carbonyl cyanide *m*-chlorophenylhydrazone (CCCP, **1**), 3Z1 (**2**), cinnamaldehyde (**3**), totarol (**4**), sanguinarine (**5**), viriditoxin (**6**), and PC190723 (**7**) (Table 1). We included cefuroxime (**8**) as a negative control as it is a therapeutic antibiotic that inhibits cell wall assembly in growing bacteria and should not perturb $\Delta\psi$ on the time scale of our experiments (*e.g.* 30 min) (Table 1). β -lactam antibiotics can depolarize bacterial membranes, but the response can take several hours depending on the antibiotic and the dosage.⁴¹

Antimicrobial and membrane potential activities of 1–8

We tested **1–8** as inhibitors of bacterial proliferation by determining their minimum inhibitory concentration (MIC) against *B. subtilis* strain 168 (Table 1). The majority of the compounds inhibited *B. subtilis* growth at μM concentrations; the exception was cinnamaldehyde, which had an MIC of 2.5 mM. We used the values of MIC to set the concentration for dosing cells and studied the resulting change in $\Delta\psi$. To determine $\Delta\psi$, we treated cells with **1–8** at $1 \times \text{MIC}$ for 5 min, exposed the cells to the membrane potential sensitive dye, 3,3'-diethyloxycarbocyanine iodide (DiOC₂) for 15 min, and measured cell fluorescence using flow cytometry. DiOC₂ is a fluorophore that emits at $\lambda_{\text{emission}} = 530$ nm in solution. When cells with a large $\Delta\psi$ are treated with DiOC₂, the fluorophore concentrates at the cell membrane, self-associates, and its emission wavelength is shifted to $\lambda_{\text{emission}} = 575$ nm. The ratio of cell fluorescence emission at $\lambda_{575}/\lambda_{530}$ nm is an indicator of $\Delta\psi$, and large values denote cells with a large intact transmembrane potential.

In a typical experiment, we measured the fluorescence intensity of $\sim 10\,000$ cells by flow cytometry. The result of compound treatment on $\Delta\psi$ is shown in Fig. 2. We used **1** as a positive control for these experiments: treating *B. subtilis* 168 cells with **1** at $1 \times \text{MIC}$ for 5 min produced a ratio of $\lambda_{575}/\lambda_{530}$ of 0.045, which indicated a large decrease in $\Delta\psi$. As a negative control, we treated *B. subtilis* cells with **8** at $1 \times \text{MIC}$ for 20 min and observed no decrease in $\Delta\psi$: $\lambda_{575}/\lambda_{530}$ was 0.306 ± 0.011 for **8** compared to 0.257 ± 0.003 for an untreated control. We found that the treatment of *B. subtilis* cells with compounds **2–5** at $1 \times \text{MIC}$ decreased $\lambda_{575}/\lambda_{530}$ indicating a significant reduction in $\Delta\psi$. FtsZ inhibitors **6** and **7** did not perturb $\lambda_{575}/\lambda_{530}$ in our assay and thus have no effect on $\Delta\psi$ within the time scale of our experiments. We also performed fluorescence controls with **1–8** only (*i.e.*, no cells) to confirm there was no competitive fluorescence emitted by **1–8** (Fig. S1A and B, ESI†). As the emission of **5** spans a region of the spectrum including λ_{575} , we performed further controls to determine the magnitude of this signal compared to the fluorescence emission from DiOC₂. We determined that the fluorescence of **5** was not significant compared to the DiOC₂ signal emitted from labelled cells under the conditions used (Fig. S2, ESI†).

Measuring the effect of 2–6 on the permeability of bacterial membranes

One mechanism by which small molecules can decrease $\Delta\psi$ is by disrupting the membrane and increasing the rate of diffusion of compounds across bilayers. We used propidium iodide (PI) to explore whether compounds **2–6** increased the permeability of *B. subtilis* membranes. PI has several characteristics that enable these measurements: (1) the cellular uptake of PI increases with increasing membrane permeability; (2) PI fluoresces upon binding to DNA ($\lambda_{\text{emission}} = 620$ nm); and (3) PI can be quantified using fluorescence microscopy or flow cytometry.⁴¹ Protonophores such as **1** decrease $\Delta\psi$, however the resulting membranes inhibit passage of solutes other than protons. Thus, PI fluorescence does not increase in cells treated with protonophores.⁴¹ This response is similar to antibiotics such as daptomycin, which increases the flux of K^+ ions across the membrane, but has no effect on PI uptake within 60 min after treatment.⁴²

We pretreated *B. subtilis* cells with compounds **1–8** at 1× MIC for 5 min, dosed cells with PI (100 μM), incubated for 30 min, and measured the fluorescence intensity at $\lambda_{\text{emission}} = 620$ nm. Fig. 3 summarizes the resulting fluorescence intensity of cells. Using the Kruskal–Wallis test, we found no significant difference between the solvent controls, **7**, and **8**. Pairwise comparison of solvent controls with **1–6** gave *p*-values of <0.001. We found that treating cells with **1** or **2** reduced their labelling with PI (compared to solvent control samples), suggesting that these compounds do not perturb membrane permeability. Instead, **1** and **2** decreased $\Delta\psi$ and eliminated the transport of the cationic fluorophore PI by the pmf. Treating *B. subtilis* 168 cells with **3–6** increased their permeability to PI. For **3–5**, we observed a decrease in $\Delta\psi$, suggesting that these compounds change global membrane properties or perturb proteins that form pores in the membrane.

As a positive control, we treated *B. subtilis* cells with 70% ethanol, rinsed cells with 1× PBS to remove ethanol, labelled cells with PI, and measured their fluorescence. The membrane permeability of these cells increased and they were extensively labelled with PI. As a control, we measured the fluorescence properties of compounds (*i.e.* no cells; Fig. S3, ESI†). As the emission of **5** spans a region of the spectrum including λ_{620} , we performed additional controls to determine if the signal would perturb the results of PI labelling. Unfortunately, the fluorescence of **5** contributed significantly in the cellular PI assay, which may account for the increase in fluorescence intensity observed (Fig. S4, ESI†).

Determining the membrane disrupting activity of **1–2**, and **4** by measuring the oxygen consumption of myoblasts

The results of DiOC₂ and PI fluorescence measurements in the presence of **2–6** indicated the compounds display two effects on bacterial membranes: (1) dissipation of $\Delta\psi$ without increasing permeability, which occurred in the presence of ionophores, including **1**; and (2) dissipation of $\Delta\psi$ and an increase in membrane permeability. We chose to study compounds **2** and **4** as they each cause one of these phenotypes. As an indication of their therapeutic potential, we determined whether these model compounds dissipated the pmf in both bacteria and eukaryotes or preferentially altered bacterial membranes. We evaluated the effect of **1**, **2**, and **4** on the oxygen consumption rate (OCR) of C2C12 myoblast cells derived from mouse muscle cell tissue. The most widely used technique for detecting changes in ΔpH across membranes is to measure the rapid increase in oxygen consumption that occurs after treatment of cells with an uncoupling agent. Treatment with an uncoupling agent enables the rapid passage of protons back into the mitochondrial matrix. Consequently, the rate of electron transport increases to restore the pmf, resulting in increased oxygen consumption. For example, treating C2C12 myoblasts with **1** caused the OCR to increase and remain higher than the basal rate (Fig. 4); we observed a maximum OCR with **1** at a concentration of 0.6 μM. Fig. S5† demonstrates all of the data points obtained for C2C12 myoblast treatment with **2** (ESI†). The addition of **2** to myoblasts also increased the OCR; we observed the maximal OCR with **2** at 30 μM. These results demonstrate that **2** causes a loss of the pmf across the inner mitochondrial membrane, suggesting that it disrupts the membrane in both prokaryotes and eukaryotes. **4** did not cause a change in the OCR relative to controls, suggesting that this compound does not uncouple the pumping of protons from ATP production in eukaryotic membranes (Fig. S6A and B, ESI†).

Although the myoblast experiments in C2C12 cells did not inform us of the mechanism by which **1**, **2**, and **4** reduce ΔpH , which may be due to influencing ion transport, membrane permeability, or *via* other mechanisms, the data demonstrates that compounds **2** and **4** are less effective at reducing $\Delta\psi$ in eukaryotes than in prokaryotes. **2** required significantly higher concentrations—compared to its MIC against *B. subtilis*—to elicit a response from

C2C12 cells. An analog of **2**—2,2'-methylenebis(4-chlorophenol), also referred to as dichlorophen—is an anthelmintic agent and has been used to treat fungal infections. Dichlorophen is tolerated in rats and has a 50% lethal dose (LD₅₀, in mg kg⁻¹ of body weight) of 1506 (95% confidence interval [CI] 1310–1760) for males and 1683 (95% CI 1402–1986) for females.⁴³ Evaluation of **2–6** in animal toxicity models would be an important step to assess their therapeutic potential.

Evaluating proton transport across the membrane of bacteria treated with **1–8**

The bacterial membrane regulates the transport of a variety of ions, including protons. To test whether **2–6** disrupted $\Delta\psi$ by functioning as protonophores, pore-forming agents, or through other membrane disruption mechanisms we studied whether these compounds relaxed ΔpH in *B. subtilis* 168 cells. Protonophores and pore-forming agents reduce the energetic barrier to proton transport across membranes and eliminate ΔpH . We assayed the protonophore activity of **1–8** by measuring the change in the external pH (ESI[†]). We created a large ΔpH in cells in a high-density culture ($\sim 3 \times 10^{10}$ cells per mL) by reducing the external pH to 6. Equilibration of the external pH with the internal pH results in an increase in the external pH value. **1** has been described as a protonophore that catalytically equilibrates ΔpH . We found that the equilibration of ΔpH by **1** was rapid.

We tested **2–6** and found their effect on cells to be similar to the solvent controls (Fig. S7A and B, ESI[†]): namely, treatment of *B. subtilis* cells with **2–6** had no significant effect on ΔpH . Only cells treated with **1** at its MIC value dissipated the artificial ΔpH . The results suggest that **2–6** are not catalytic protonophores in contrast to **1**, which transports protons across the membrane. Although the artificial ΔpH was not equilibrated by **2–6**, it remains possible that the ΔpH and $\Delta\psi$ of these cells decreased and was not detectable in our experiments. Another limitation may be the significant difference in the amount of membrane present in the ΔpH experiments ($\sim 3 \times 10$ cells per mL) compared to MIC or DiOC₂ and PI labelling experiments ($\sim 5 \times 10^5$ or $\sim 1 \times 10^8$ cells per mL). The activity of **2–6** may require a threshold lipid-to-inhibitor ratio before the effect is observed. The addition of **2** to *B. subtilis* cells at a concentration that increased the OCR in C2C12 myoblasts (30 μM , ~ 200 times greater than its MIC) equilibrated the artificial ΔpH (Fig. S6B, ESI[†]). Our observation that a high concentration of **2** is required to observe the relaxation of the ΔpH may suggest a relationship between the concentration of lipids and the activity of this compound *in vivo*.

Mislocalization of membrane-associated proteins in cells by **2–6**

Having established that **2–5** reduced $\Delta\psi$ and **3–6** increased the membrane permeability of *B. subtilis* cells, we were interested in whether these physiological changes mislocalized membrane-associated proteins. Significant fluorescence interference from **5** prevented us from including **5** in the localization study (Fig. S8, ESI[†]). The distribution of GFP-MinD in *B. subtilis* cells treated with **1–4** and **6** resulted in reduction of localized MinD fluorescence, as shown in Fig. 5. Treatment of cells with **7** and **8** resulted in localization of MinD and was consistent with controls. This result suggests that depletion of $\Delta\psi$ and/or increasing membrane permeability with **2–6** mislocalizes proteins that are positioned at membranes, such as FtsZ. MinD localization in *E. coli* is dynamic and has a time-averaged position at the poles. Treatment of *E. coli* cells with **1** or **2** resulted in a change in the distribution of MinD relative to the normal time-averaged polar localization with DMSO treatment, as shown in Fig. 6. The addition of **1** resulted in the diffusion of MinD fluorescent signal throughout the cell. Treatment of cells with **2** reduced the number of MinD foci and increased the dispersion of the fluorescent protein throughout many of the cells. Although **2–6** are described as FtsZ inhibitors, they display a broad range of effects *in vivo* that are consistent with membrane activity, rather than a specific effect on FtsZ. This activity results in the

delocalization of membrane-associated proteins, which perturbs pathways involved in division and cell shape and may be ultimately responsible for the phenotypes observed *in vivo*.

Conclusions

The activity of ionophores, permeabilizing agents, and molecules that dissipate $\Delta\psi$ perturb the localization of important bacterial cell shape and division proteins. These proteins rely on $\Delta\psi$ for their localization and function *in vivo*.¹⁰ Significant effects on cell division and morphology should be expected to accompany changes in $\Delta\psi$. Although **2–6** are not specific FtsZ inhibitors *in vivo*, studies of their function can contribute to an understanding how membrane active compounds disrupt cellular physiology. Our results indicate that dissipation of $\Delta\psi$ is an important phenotype for evaluating inhibitors of FtsZ and other membrane-associated proteins. The mislocalization of these proteins may cause a misinterpretation of the mechanism of action of these compounds *in vivo*. This effect is particularly germane if the compounds are applied to studying proteins in live cells. These studies provide a foundation for testing inhibitors of proteins that regulate bacterial cell shape and division for membrane activity to reveal their real targets *in vivo*.

Materials and methods

Determination of antimicrobial susceptibility

We grew bacteria using the conditions in parenthesis to determine minimum inhibitory concentrations (MICs): *E. coli* strain MG1655 wildtype strain (Luria-Bertani [LB] media, 30 °C, 200 rpm shaking, 14 h) and *B. subtilis* strain 168 (LB media, 37 °C, 200 rpm shaking, 16 h). We diluted cultures to 5×10^5 cells per mL in growth media for the starting inoculum. The compounds tested include carbonyl cyanide *m*-chlorophenylhydrazone (CCCP, **1**), zantrin 3Z1 (**2**), cinnamaldehyde (**3**), totarol (**4**), sanguinarine (**5**), viriditoxin (**6**), PC190723 (**7**), and cefuroxime (**8**). Compounds **1** (97%), **3** (99%), **5** (98%), and **8** (99%) were from Sigma with the purity indicated in parenthesis. We synthesized **2**, **4**, **6**, and **7** according to previously published methods.^{44–47} We dissolved compounds in DMSO with the exception of sanguinarine, which we dissolved in methanol.

We performed MIC measurements using the macro-dilution technique according to the NCCLS guidelines.⁴⁸ To create a two-fold dilution series for the macrodilution technique, we added each compound to the first culture tube (4 mL total volume) at the highest concentration. We diluted 2 mL of this culture into an equal volume of inoculated media (a two-fold dilution). The final volume for each culture was 2 mL. We prepared solvent controls and sterility controls using the same concentration of solvent as the tubes containing the highest concentration of antibiotic. We determined the macrodilution MIC endpoints in triplicate by identifying the lowest concentration of compound that completely inhibited growth by visual inspection.

Flow cytometry, DiOC₂ labeling, propidium iodide labeling

We used flow cytometry to measure the extent of membrane potential depletion. DiOC₂ associated with membranes exhibits red fluorescence ($\lambda_{\text{excitation}} = 488 \text{ nm}$, $\lambda_{\text{emission}} = 575 \text{ nm}$), whereas cytosolic DiOC₂ has green fluorescence ($\lambda_{\text{excitation}} = 488 \text{ nm}$, $\lambda_{\text{emission}} = 530 \text{ nm}$). The depletion of $\Delta\psi$ reduces the concentration of DiOC₂ associated with the membrane and decreases the $\lambda_{575}/\lambda_{530}$ ratio of DiOC₂. We measured the ratio of $\lambda_{575}/\lambda_{530}$ using flow cytometry. We filtered cell suspensions labelled with 30 μM DiOC₂ through a Nylon filter containing 60 μm diameter pores. For each sample, we acquired 10 000 data points using a BD LSRII flow cytometer and analyzed the data using FlowJo v7.6.4. We

also used flow cytometry to measure the permeability of the membrane using 100 μM PI. PI is impermeable to cells with intact membranes regardless of $\Delta\psi$.⁴¹ PI diffuses into cells that have disrupted membranes, binds DNA, and produces a fluorescent DNA-PI complex ($\lambda_{\text{excitation}} = 488 \text{ nm}$, $\lambda_{\text{emission}} = 620 \text{ nm}$). We performed pair-wise comparison of PI data sets by the Kruskal–Wallis test using the program GraphPad InStat 3.

Oxygen consumption in myoblasts treated with 1, 2, and 4

We measured the OCR using a Seahorse Biosciences XF96 Extracellular Flux Analyzer as previously described with minor alterations.⁴⁹ We seeded C2C12 mouse myoblasts in XF96 cell culture microplates (Seahorse Biosciences) at 12 000 cells per well in DMEM high glucose medium (Invitrogen) containing 10% FBS, 100 units per mL penicillin, and 100 $\mu\text{g mL}^{-1}$ streptomycin and incubated the cells at 37 °C and 5% CO_2 for approximately 18 h. Prior to measurements, we exchanged the growth media for XF Assay Medium (Seahorse Biosciences) supplemented with 25 mM glucose (Sigma) and incubated the plate at 37 °C for 60 min. We preloaded compounds dissolved in nutrient media to the reservoirs and injected these solutions into the assay wells during experiments. OCR measurements consisted of a 3 min mixing period followed by the measurement of oxygen consumption over a 5 min time interval.

Fluorescence microscopy of fusion proteins sensitive to $\Delta\psi$

We grew *B. subtilis* DS4294 ($\text{amyE}::\text{P}_{\text{xyI}}\text{-gfp-minD}$, cat^{R}) to exponential phase ($\lambda = 600 \text{ nm}$, 0.4–0.7) in LB with incubation at 30 °C and 200 rpm shaking. We diluted cultures with LB to a $\lambda = 600 \text{ nm}$ of 0.4 and induced GFP-MinD production by adding xylose to the media to a final concentration of 0.1% (w/v) followed by incubating for 75 min. After induction, we treated cells with **1–8** at 1 \times MIC concentration or DMSO solvent controls for 20 min before imaging. We pipetted suspensions of treated cells on 1% (w/v) agarose pads containing 1 \times phosphate buffered saline (PBS) infused with **1–8** at 1 \times MIC or DMSO. We performed epifluorescence microscopy on a Nikon Eclipse TE2000-E microscope equipped with PFS using a Nikon Plan Apo 100 \times /1.40 phase contrast oil objective, a 1.5 \times optivar, and an Andor iXon^{EM} CCD camera. We imaged cells with phase contrast and fluorescence at an excitation $\lambda = 484 \text{ nm}$ and emission $\lambda = 520 \text{ nm}$ using an EXFO X-cite[®] series 120 lamp and collected data using MetaMorph software (version 7.5.6.0, MDS Analytical Technologies). We imaged cells from at least three separate induction experiments for each compound; we also performed controls using DMSO (negative control) and **1** (positive control) for each induction. After transferring the cells to agarose pads, we imaged cells within 10 min.

We grew *E. coli* MG1655 pFX9 ($\text{P}_{\text{lac}}\text{-gfp-minD-minE}$) to early exponential phase ($\lambda = 600$, 0.3–0.4) in LB with incubation at 30 °C and 200 rpm shaking. We induced GFP-MinD and MinE production by adding IPTG to the media to a final concentration of 50 μM and incubating for 75 min. We treated induced cells with a 1 \times MIC concentration of **1**, **2**, or DMSO solvent for 20 min before imaging. We pipetted suspensions of treated cells on 1% (w/v) agarose pads infused with 1 \times PBS containing **1** or **2** at their 1 \times MIC value (or DMSO). We imaged cells from at least three separate induction experiments for **1**, **2**, and DMSO. After transferring the cells to agarose pads, we imaged cells within 10 min.

Image analysis to evaluate fluorescent protein localization in cells treated with 1–8

We grouped phase contrast and fluorescence images for data analysis using the MicrobeTracker Suite (version 0.930, Emonet Lab, Jacobs-Wagner Lab; Yale University) running in MAT-LAB (version 7.13.0.564 R2011b, Mathworks). We used MicrobeTracker to define the outer edge of the cells. We corrected background fluorescence signal for each cell using a line scan with the cell segmented into ~ 1 pixel steps. We processed line scan

data with a custom MATLAB script. The script first normalized the fluorescence signal for the area of each segment. Cell segments were ordered such that the brightest half of the cell (corrected fluorescence) had the first segment number. To find peaks in the corrected fluorescence signal for *B. subtilis* cells, we used the PeakFinder MATLAB script.⁵⁰ We recorded peak locations as percent of cell length by dividing the segment number for the peak by the total segments for the respective cell. We analyzed the concatenated data sets to compare the distribution of fluorescent peaks for each set of experimental conditions. We performed Fisher's exact test using the two categories (*i.e.*, cells with localization and cells without localization) to obtain *p*-values for the comparison of DMSO or **1–8** treated *B. subtilis* cells. To evaluate the localization of MinD in *E. coli* cells treated with compounds, we divided the cell into 100 segments (*i.e.* bins) to generate histograms. We assigned the corrected fluorescence signal of each segment to each respective bin. We calculated bins overlapping two segments by summing the fractions of the adjacent segments. Using this approach, we analyzed the fluorescence distribution for cells treated with different compounds.

Supplementary Material

Refer to Web version on PubMed Central for supplementary material.

Acknowledgments

We thank Prof. Daniel Kearns for *B. subtilis* strain DS4294. We acknowledge the Human Frontiers Science Program (RGY0069/2008-C103), USDA (WIS01192), NIH (1DP2OD008735-01), and an Alfred P. Sloan Research Fellowship (D.B.W.) for funding this research. C.I.G., N.A.S., and J.T.S. acknowledge research support from NIH/NIAID (R01AI08093).

References

1. Bi EF, Lutkenhaus J. *Nature*. 1991; 354:161–164. [PubMed: 1944597]
2. Addinall SG, Cao C, Lutkenhaus J. *J Bacteriol*. 1997; 179:4277–4284. [PubMed: 9209044]
3. Wang Y, Jones BD, Brun YV. *Mol Microbiol*. 2001; 40:347–360. [PubMed: 11309118]
4. Weart RB, Lee AH, Chien AC, Haeusser DP, Hill NS, Levin PA. *Cell*. 2007; 130:335–347. [PubMed: 17662947]
5. Michel B. *PLoS Biol*. 2005; 3:e255. [PubMed: 16000023]
6. Janion C. *Int J Biol Sci*. 2008; 4:338–344. [PubMed: 18825275]
7. Bernhardt TG, de Boer PA. *Mol Cell*. 2005; 18:555–564. [PubMed: 15916962]
8. Wu LJ, Ishikawa S, Kawai Y, Oshima T, Ogasawara N, Errington J. *EMBO J*. 2009; 28:1940–1952. [PubMed: 19494834]
9. Handler AA, Lim JE, Losick R. *Mol Microbiol*. 2008; 68:588–599. [PubMed: 18284588]
10. Strahl H, Hamoen LW. *Proc Natl Acad Sci U S A*. 2010; 107:12281–12286. [PubMed: 20566861]
11. Ehrenberg B, Montana V, Wei MD, Wuskell JP, Loew LM. *Biophys J*. 1988; 53:785–794. [PubMed: 3390520]
12. Breeuwer, P.; Abee, T. *Assessment of the Membrane Potential, Intracellular pH and Respiration of Bacteria Employing Fluorescence Techniques*. Kluwer Academic Publishers; 2004.
13. Margalit DN, Romberg L, Mets RB, Hebert AM, Mitchison TJ, Kirschner MW, RayChaudhuri D. *Proc Natl Acad Sci U S A*. 2004; 101:11821–11826. [PubMed: 15289600]
14. Domadia P, Swarup S, Bhunia A, Sivaraman J, Dasgupta D. *Biochem Pharmacol*. 2007; 74:831–840. [PubMed: 17662960]
15. Jaiswal R, Beuria TK, Mohan R, Mahajan SK, Panda D. *Biochemistry*. 2007; 46:4211–4220. [PubMed: 17348691]
16. Beuria TK, Santra MK, Panda D. *Biochemistry*. 2005; 44:16584–16593. [PubMed: 16342949]

17. Wang J, Galgoci A, Kodali S, Herath KB, Jayasuriya H, Dorso K, Vicente F, Gonzalez A, Cully D, Bramhill D, Singh S. *J Biol Chem*. 2003; 278:44424–44428. [PubMed: 12952956]
18. Adams DW, Wu LJ, Czaplewski LG, Errington J. *Mol Microbiol*. 2011; 80:68–84. [PubMed: 21276094]
19. Rai D, Singh JK, Roy N, Panda D. *Biochem J*. 2008; 410:147–155. [PubMed: 17953519]
20. Beuria TK, Singh P, Surolia A, Panda D. *Biochem J*. 2009; 423:61–69. [PubMed: 19583568]
21. Foss MH, Eun YJ, Weibel DB. *Biochemistry*. 2011; 50:7719–7734. [PubMed: 21823588]
22. Foss MH, Weibel DB. *Antimicrob Agents Chemother*. 2010; 54:3988–3990. [PubMed: 20566769]
23. Ingolfsson HI, Koeppe RE 2nd, Andersen OS. *Biochemistry*. 2007; 46:10384–10391. [PubMed: 17705403]
24. Hung WC, Chen FY, Lee CC, Sun Y, Lee MT, Huang HW. *Biophys J*. 2008; 94:4331–4338. [PubMed: 18310254]
25. Smith EC, Kaatz GW, Seo SM, Wareham N, Williamson EM, Gibbons S. *Antimicrob Agents Chemother*. 2007; 51:4480–4483. [PubMed: 17664318]
26. Haraguchi H, Oike S, Muroi H, Kubo I. *Planta Med*. 1996; 62:122–125. [PubMed: 8657742]
27. Micol V, Mateo CR, Shapiro S, Aranda FJ, Villalain J. *Biochim Biophys Acta*. 2001; 1511:281–290. [PubMed: 11286971]
28. Mateo CR, Prieto M, Micol V, Shapiro S, Villalain J. *Biochim Biophys Acta*. 2000; 1509:167–175. [PubMed: 11118528]
29. Seifen E, Adams RJ, Riemer RK. *Eur J Pharmacol*. 1979; 60:373–377. [PubMed: 230984]
30. Serafim TL, Matos JA, Sardao VA, Pereira GC, Branco AF, Pereira SL, Parke D, Perkins EL, Moreno AJ, Holy J, Oliveira PJ. *Biochem Pharmacol*. 2008; 76:1459–1475. [PubMed: 18692024]
31. Wong DT, Hamill RL. *Biochem Biophys Res Commun*. 1976; 71:332–338. [PubMed: 134706]
32. Nicholas RA, Ordal GW. *Biochem J*. 1978; 176:639–647. [PubMed: 106840]
33. Terada H. *Environ Health Perspect*. 1990; 87:213–218. [PubMed: 2176586]
34. Hurdle JG, O'Neill AJ, Chopra I, Lee RE. *Nat Rev Microbiol*. 2011; 9:62–75. [PubMed: 21164535]
35. Ejim L, Farha MA, Falconer SB, Wildenhain J, Coombes BK, Tyers M, Brown ED, Wright GD. *Nat Chem Biol*. 2011; 7:348–350. [PubMed: 21516114]
36. Rothfield L, Taghbalout A, Shih YL. *Nat Rev Microbiol*. 2005; 3:959–968. [PubMed: 16322744]
37. Hu Z, Lutkenhaus J. *Mol Microbiol*. 1999; 34:82–90. [PubMed: 10540287]
38. Hu Z, Lutkenhaus J. *Mol Microbiol*. 2003; 47:345–355. [PubMed: 12519187]
39. Mileykovskaya E, Fishov I, Fu X, Corbin BD, Margolin W, Dowhan W. *J Biol Chem*. 2003; 278:22193–22198. [PubMed: 12676941]
40. Renner LD, Weibel DB. *Proc Natl Acad Sci U S A*. 2011; 108:6264–6269. [PubMed: 21444798]
41. Novo DJ, Perlmutter NG, Hunt RH, Shapiro HM. *Antimicrob Agents Chemother*. 2000; 44:827–834. [PubMed: 10722477]
42. Silverman JA, Perlmutter NG, Shapiro HM. *Antimicrob Agents Chemother*. 2003; 47:2538–2544. [PubMed: 12878516]
43. Gaines TB, Linder RE. *Fundam Appl Toxicol*. 1986; 7:299–308. [PubMed: 3758548]
44. Sorto NA, Olmstead MM, Shaw JT. *J Org Chem*. 2010; 75:7946–7949.
45. Park YS, Grove CI, Gonzalez-Lopez M, Uргаonkar S, Fettinger JC, Shaw JT. *Angew Chem Int Ed*. 2011; 50:3730–3733.
46. Kim MB, Shaw JT. *Org Lett*. 2010; 12:3324–3327. [PubMed: 20597470]
47. Moshfegh AA, Mazandarani B, Nahid A, Hakimelahi GH. *Helv Chim Acta*. 1982; 65:1229–1232.
48. NCCLS. National Committee for Clinical Laboratory Standards. Vol. 20. Wayne, PA: 2000.
49. Nicholls DG, Darley-Usmar VM, Wu M, Jensen PB, Rogers GW, Ferrick DA. *J Visualized Exp*. 2010:e2511.
50. Yoder N. MATLAB Central. Jun 14.2011

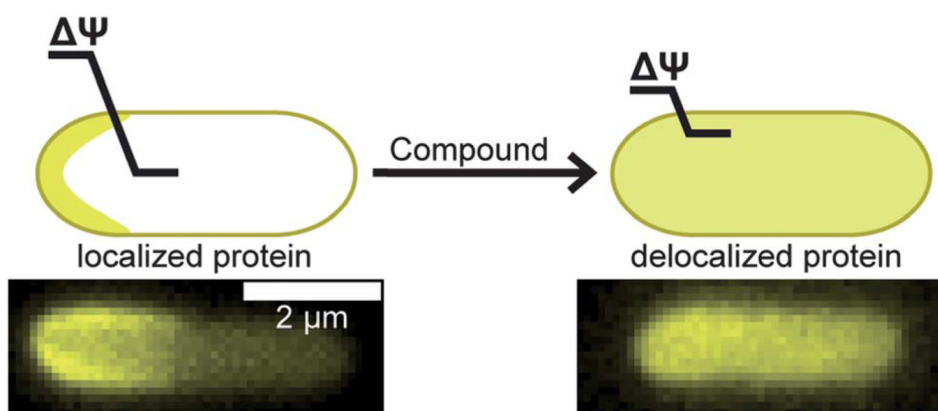


Fig. 1. The loss of $\Delta\psi$ disrupts the normal localization pattern of membrane-associated proteins. The cartoon depicts the diffuse pattern of a polarly localized protein after reduction of $\Delta\psi$. The length of the line across the membrane depicts the relative magnitude of $\Delta\psi$. Fluorescence images below the cartoon represent MinD localization in *E. coli* cells with DMSO treatment on the left and **1** treatment on right. The scale bar represents 2 μm .

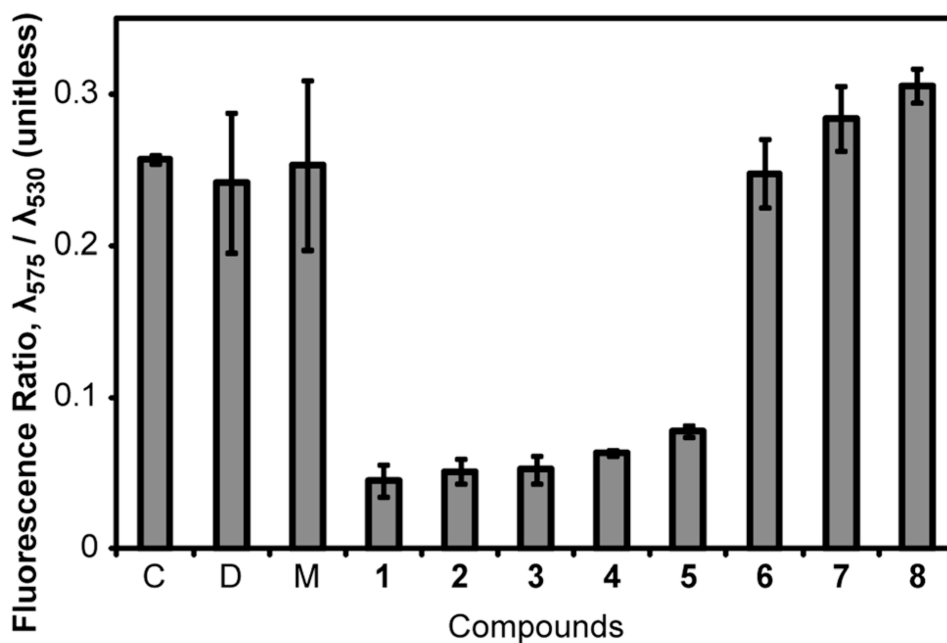


Fig. 2. Measurement of the perturbation of $\Delta\psi$ of *B. subtilis* 168 cells by compounds 1–8. We determined the relative magnitude of $\Delta\psi$ of *B. subtilis* 168 cells by measuring the $\lambda_{575}/\lambda_{530}$ fluorescence emission intensity ratio of DiOC₂ after excitation at λ_{488} . A large value of $\lambda_{575}/\lambda_{530}$ represents a high $\Delta\psi$. Labels ‘C’, ‘D’, and ‘M’ stand for control (untreated), DMSO, and methanol, respectively. Error bars represent two standard deviations from the mean ($n = 3$).

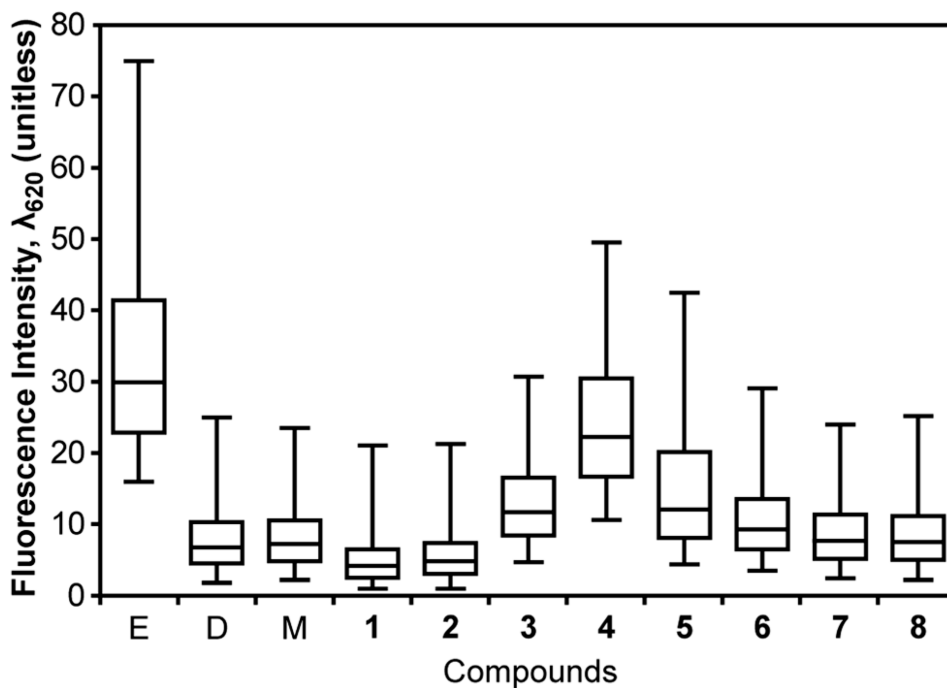


Fig. 3. Effect of **1–8** on the integrity of *B. subtilis* 168 cell membranes. We measured the permeability of the cell membrane to PI by labeling *B. subtilis* 168 cells after treatment with compounds. We measured PI fluorescence intensity at λ_{620} . Large values of fluorescence intensity represent an increasing membrane permeability to PI. Labels ‘E’, ‘D’, and ‘M’ stand for ethanol, DMSO, and methanol, respectively. Whisker plots display the median (center of the box), 25 to 75% of the population in the box, and 5 to 95% of the population between the outer whiskers.

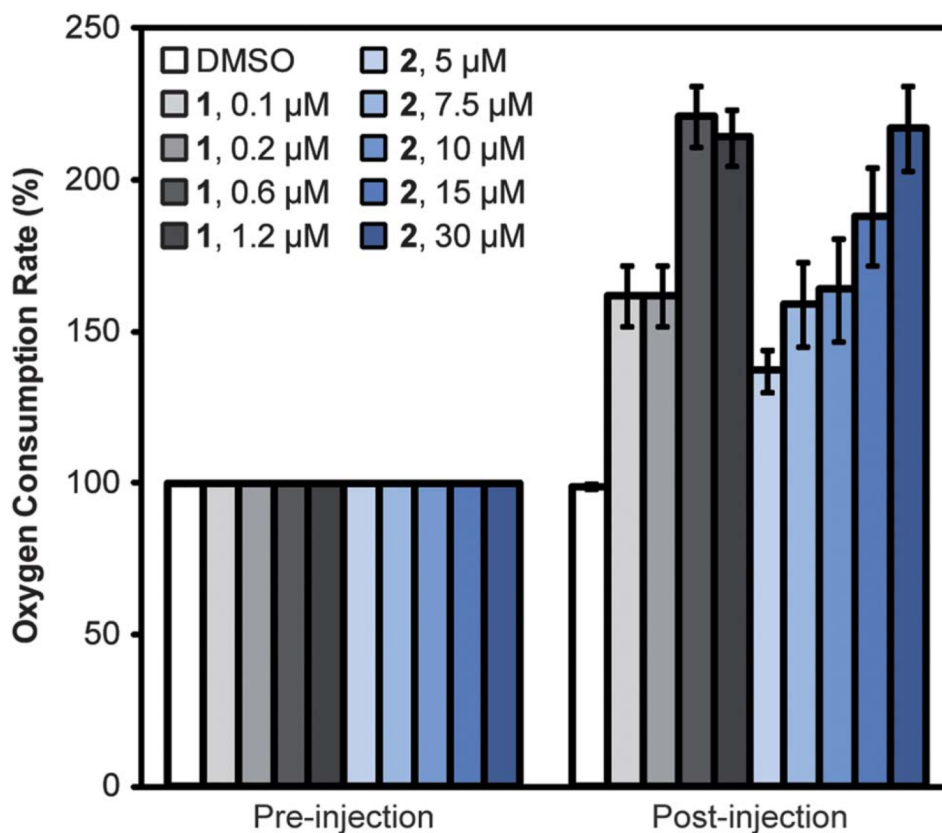


Fig. 4. Measurement of the uncoupling activity of **1** and **2** in C2C12 myoblasts. We measured the OCR of C2C12 myoblasts before and after injection of **1**, **2**, or DMSO (the solvent control). The addition of protonophore **1** increased the OCR of C2C12 myoblasts. The addition of **2** also resulted in a rise in OCR, consistent with a depletion of the pmf. The maximum OCR was achieved at 0.6 μM of **1** and 30 μM of **2**. Error bars represent two standard deviations of the mean ($n = 8$).

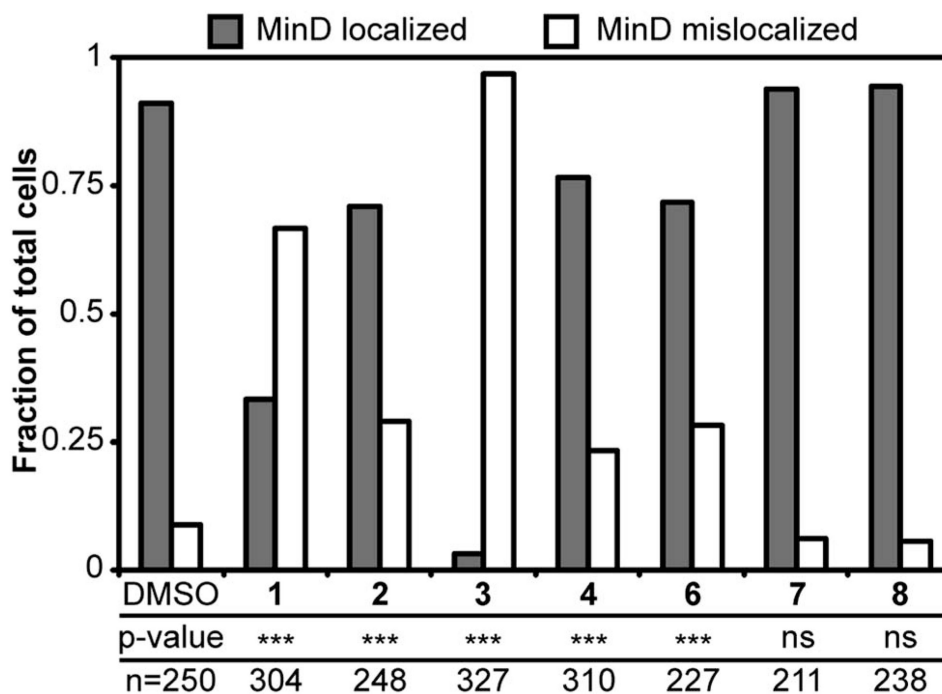


Fig. 5.

Localization of MinD in *B. subtilis* cells treated with 1–8. Grey bars and white bars represent cells with MinD localization and without MinD localization, respectively. The addition of 1–6 reduced the localization of MinD. Localization of MinD to the poles and the midcell of dividing cells remained normal in the DMSO solvent control. *P*-values from a Fisher's exact test comparing DMSO with treatments are represented as *** for $p < 0.001$ and ns as not significant. The *p*-values for 7 and 8 are 0.3778 and 0.1644, respectively. The number of cells analyzed in each treatment is listed as '*n*'.

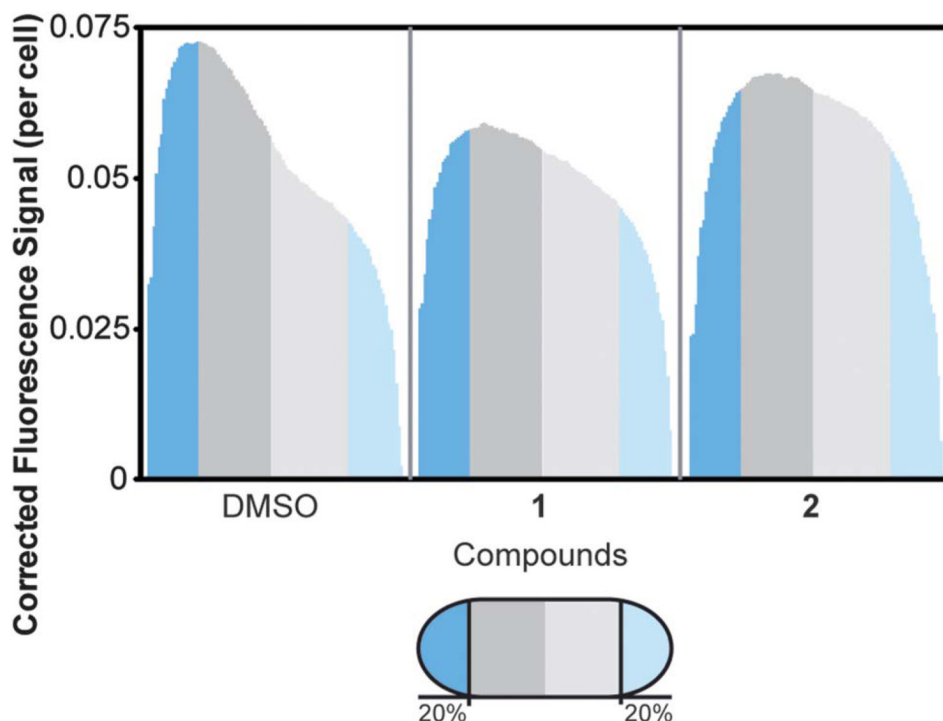
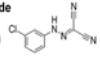
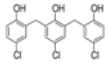
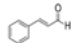
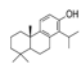
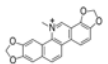
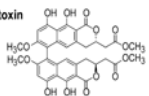
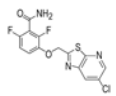
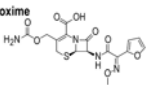


Fig. 6. Distribution of MinD in *E. coli* cells following treatment with **1** or **2**. We normalized the cell length to average the distribution of fluorescence. The cells were organized with the brightest half of the cell oriented on the left. The normalized cell length is shown in 100 divisions, with the first and last 20% of cell length labeled in blue. The remainder of the cell is divided in half by dark and light grey segments. The number of cells assayed for each treatment is as follows: DMSO ($n = 123$), **1** ($n = 111$), and **2** ($n = 147$). The addition of **1** resulted in diffuse MinD localization throughout the cell, as opposed to the time-averaged polar localization observed in the DMSO solvent control. Addition of **2** also resulted in a significant reduction in the dynamic localization of MinD to the poles; the fluorescence of the resulting cells was disperse.

Table 1
The structures and minimum inhibitory concentrations (MICs) of compounds 1–8 against *B. subtilis* strain 168

Inhibitor structure	MIC
1 - Carbonyl cyanide m-chlorophenyl hydrazone (CCCP) 	10 μ M
2 - Zantrin Z1 	0.16 μ M
3 - Cinnamaldehyde 	2.5 mM
4 - Totarol 	2.5 μ M
5 - Sanguinarine 	10 μ M
6 - Viriditoxin 	0.63 μ M
7 - PC190723 	2.5 μ M
8 - Cefuroxime 	20 μ M